NUMERICAL INVESTIGATION ON THE SOLIDS MIXING IN FLUIDIZED BEDS

F. Hernández-Jiménez[1*], J. Sánchez-Prieto[1], A. Soria-Verdugo[1], E. Cano-Pleite[1], A. Acosta-Iborra[1]

[1]*Department of Thermal and Fluid Engineering, Carlos III University of Madrid, SPAIN*

*Email: *fhjimene@ing.uc3m.es*

Abstract – The present work aims to study the mixing mechanisms in fluidized beds by means of numerical simulations. The two-fluid model (TFM) available in MFIX code is selected to carry out the numerical simulations. The numerical results are compared with experiments obtained in a pseudo-2D fluidized bed that allows optical access to the interior of the system through a frontal glass wall. The experiments were performed by placing particles of equal characteristics but of different color in two vertical layers. In the TFM three phases are defined, one for the gas phase and two for each of the solids phases to be mixed. To improve the simulation prediction, a friction model accounting for the front and rear walls effect on the continuum solid phases was introduced in the TFM. This friction model leads to simulation results closer to the experiments. Mixing times of the same order are found in the simulations and the experiments when analyzing the mixing process macroscopically. Furthermore, the simulations are employed to analyze the mixing in the fluidized bed using a more detailed mixing index allowed by the discrimination of the three phases.

INTRODUCTION

The basic mechanism of solids mixing in bubbling fluidized beds is relatively well understood. When a bubble rises through the bed, it conveys a wake of particles to the bed surface. This is compensated by a downflow of solids in the region surrounding the rising bubble, resulting on an overall convective circulation of particles in the axial direction of the bed. At the same time, a lateral mixing of solids occurs, which is partly caused by the lateral motion of bubbles and by the lateral dispersion of particles in the bubble wake at the bed surface (Rhodes et al., 2001).

The lateral mixing of solids has been extensively characterized by means of the lateral dispersion coefficient, typically obtained from particle tracking experiments. The overall solids mixing process in fluidized beds has been also studied by mixing particles with the same properties but with different colors. It is generally assumed that the solids mixing rate in a fluidized bed can be modeled as an exponential function (i.e. Lacey mixing index (Lacey, 1954)). Besides, the lateral dispersion coefficient is a parameter in the 1D diffusion equation (Fick's law), which has also an exponential term for the analytical solution of this particular case.

Besides, numerical simulations, either using Eulerian–Eulerian two-fluid models (TFM) and Eulerian–Lagrangian approaches, such as discrete element models (CFD-DEM), can be a very effective complementary tool to experiments for achieving a detailed analysis of the hydrodynamics of complex gas–solids flows. The CFD-DEM strategy is based on a Lagrangian simulation of each particle trajectory coupled with an Eulerian simulation of the bulk gas flow. The gas–solid interaction is computed through semi-empirical closure models to reduce the level of detail required in the solution of the gas phase. In the TFM approach, the gas phase and the solid phase are treated as two interpenetrating and continuum media in an Eulerian framework using the conservation equations of the different phases. Therefore, TFM simulations are currently the most suitable strategy for the simulation of both the macro- and meso-scales of the bed when the number of particles involved is high. This allows the simulation of medium and moderately-large sized beds commonly used in laboratory research and pilot plant testing.

The present work aims to study the different mixing mechanisms in fluidized beds by means of numerical simulations. The MFIX-TFM code was selected to carry out the numerical simulations (Syamlal et al., 1993, Benyahia et al., 2007). The numerical results were compared with experiments obtained in a pseudo-2D fluidized bed that allows optical access to the interior of the system through the frontal glass wall.

The experiments were performed by placing particles of the same properties but with different color (black and white) in two vertical layers (Sánchez-Prieto et al., 2017). Then, the fluidization gas (air) was suddenly introduced through the distributor of the bed while the frontal images of the bed are recorded. The mixing process, as well as the lateral dispersion coefficient, can be estimated using the time evolution of a mixing index.

The same methodology used in the experiments was employed in the TFM simulations. In this case, three phases were defined in the TFM: one for the gas phase and two for the white and black solids phases to be mixed. The two solid phases were identical, as in the experiments, but were defined separately in the simulation to make them distinguishable. Furthermore, to improve the simulation prediction, a friction model accounting for the front and rear walls effect on the continuum solid phase was introduced in the TFM (Hernández-Jimenez et al., 2016). This model allows for the simulation of the pseudo-2D bed using a standard 2D domain instead of a more computationally demanding 3D domain.

EXPERIMENTAL SETUP

The experimental facility employed in this work is a pseudo-2D cold fluidized bed of dimensions 0.3 m x 1 m x 0.01 m. The gas distributor consists of a perforated plate with two rows of 30 holes of 1 mm diameter arranged in a triangular configuration with 1 cm pitch. A schematic diagram of the experimental setup is shown in Figure 1. The bed was filled with ballotini glass particles of 2500 kg/m^3 density. The experiments were carried out for three different particle sizes of 0.4–0.6 mm, 0.6–0.8 mm and 1–1.3 mm diameter. The tracer particles employed were a fraction of the ballotini glass particles painted in black. The black coating is thin enough to consider that the physical properties of the particles (shape, size and density) are the same as the non-painted (white) particles.

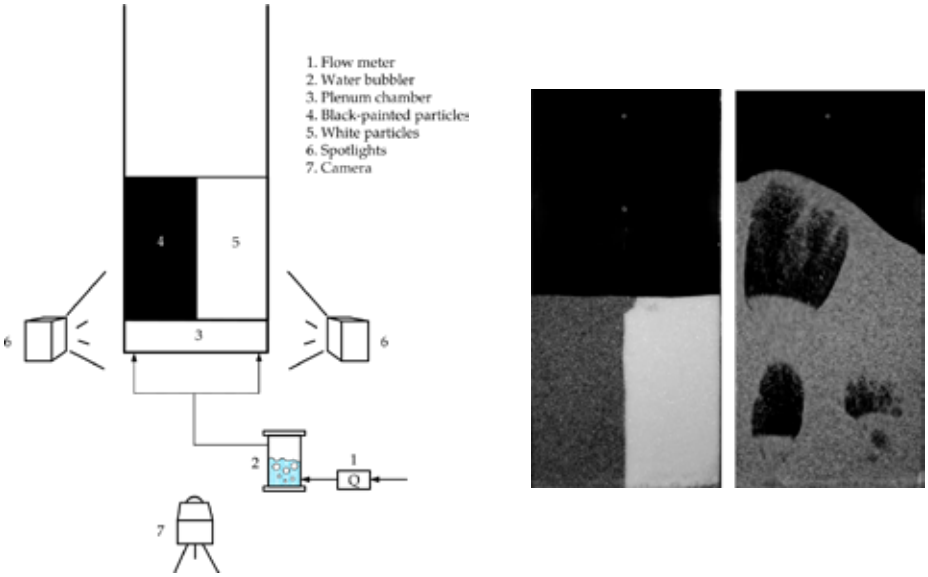

(a) (b)

Fig. 1. (a) Schematic diagram of the experimental setup and (b) examples of the completely laterally segregated state and randomly mixed state.

The air flow was measured with a set of two flow meters, with ranges of 0–200 L/min and 0–500 L/min providing an accuracy of 1% of full-scale span (FSS), which means a measurement uncertainty of 2 and 5 l/min respectively. The front and rear walls of the bed were made of glass and the rear wall was painted in black to increase contrast in the front image. A Nikon standard digital camera was used to record images of the front wall of the fluidized bed at 60 fps with a spatial resolution o 720 x 1280 pixels.

In each experiment, a removable partition was firstly inserted vertically in the center of the bed to divide it into two equal parts (Figure 1b). One side was filled with the black painted particles and the other side with the original non-painted particles. The bed aspect ratio was $H_0/W=1$ in all the cases. After that, the partition was carefully removed to not mix the particles laterally and the fluidizing air supply was turned on at the desired gas superficial velocity while the bed frontal view was recorded with the digital camera. At the end of the experiment, the particles of both colors were randomly mixed. The effect of the gas superficial velocity and the particle size on the solids mixing process in fluidized beds were analyzed. To do that, three different particle sizes and gas velocities were tested, keeping constant the bed aspect ratio. A summary of the different experiments conducted is shown in Table 1.

Table.1: Experiments.

Particle size (mm)	U_{mf} (m/s)	U_0-U_{mf} (m/s)		
0.4 – 0.6	0.27	0.27	0.40	0.54
0.6 – 0.8	0.44	0.44	0.66	0.88
1 – 1.3	0.67	0.67	1.00	1.34

EXPERIMENTAL DATA PROCESSING

Every image of the experiment was processed Digital Image Analysis (DIA). The processing consists on estimating the rate of disappearance of the white area. In this procedure, the initial state has the theoretical maximum white area. The final state is reached when no white area is detected in the images because mixing of black and white particles has completely reached the pixel scale (Otsu, 1979) leading to a grey color. The grey region is recognized in this case as black region once the images are binarized

The Lacey index is usually applied to estimate the mixing index of binary samples. In this work, the black solid phase and the bubble phase cannot be differentiated in the images because the bed rear wall is also black. Therefore, a modified mixing index is defined in Eq. (1), based on Lacey index.

$$MI = 1 - \frac{A_{w,i}}{A_{w,\max}} \tag{1}$$

where $A_{w,i}$ is the area of the white region of the binarized image i and $A_{w,max}$ is the maximum area of the white region detected in all the sequence of images, which corresponds to a state where the bed has reached the maximum bed expansion at the beginning of the experiment.

NUMERICAL SIMULATIONS

The open-source MFIX-TFM code, developed at US Department of Energy's National Energy Technology Laboratory, was used to conduct the numerical simulations. In the MFIX-TFM code, the Eulerian–Eulerian continuum description of the gas and dense phases (i.e. two-fluid model) is based on the conservation equations of mass, momentum and the balance equation of granular temperature (Benyahia et al., 2007 and Syamlal et al., 1993). The kinetic theory of granular flow, which characterizes the stochastic fluctuations of the solids kinetic energy, was used for the closure of the solids stress terms. The closure expressions for the Eulerian–Eulerian model can be found in Benyahia et al. (2007).

The governing equations of the two-fluid model, applied to a mesh of 62 x 202 square cells (5 mm length) in a 2D domain representing a vertical section of the pseudo-2D bed, are summarized in the following lines.

The numerical simulations account for the particles of different colors by defining two solid phases of identical properties and governing equations. One solid phase is defined for the white solids (s_1) and the other for the black solids (s_2).

$$\alpha_g + \alpha_{s1} + \alpha_{s2} = 1 \tag{2}$$

Mass conservation of the gas (g) and solids (s) phases:

$$\frac{\partial}{\partial t}\left(\alpha_g \rho_g\right) + \nabla \cdot \left(\alpha_g \rho_g \vec{v}_g\right) = 0 \tag{3}$$

$$\frac{\partial}{\partial t}\left(\alpha_s \rho_s\right) + \nabla \cdot \left(\alpha_s \rho_s \vec{v}_s\right) = 0 \tag{4}$$

Momentum conservation of the gas and solids phases:

$$\frac{\partial}{\partial t}\left(\alpha_g \rho_g \vec{v}_g\right) + \nabla \cdot \left(\alpha_g \rho_g \vec{v}_g \vec{v}_g\right) = -\alpha_g \nabla p + \nabla \cdot \bar{\bar{\tau}}_g + \alpha_g \rho_g \vec{g} - K_{gs}\left(\vec{v}_g - \vec{v}_s\right) \tag{5}$$

$$\frac{\partial}{\partial t}\left(\alpha_s \rho_s \vec{v}_s\right) + \nabla \cdot \left(\alpha_s \rho_s \vec{v}_s \vec{v}_s\right) = -\alpha_s \nabla p + \nabla \cdot \bar{\bar{\tau}}_s - \nabla p_s + \alpha_s \rho_s \vec{g} + K_{gs}\left(\vec{v}_g - \vec{v}_s\right) - \vec{f}_{fric} \tag{6}$$

The balance for the granular temperature, Θ, is:

$$\frac{3}{2}\left(\frac{\partial}{\partial t}\left(\alpha_s \rho_s \Theta\right) + \nabla \cdot \left(\alpha_s \rho_s \vec{v}_s \Theta\right) = -\left(p_s \bar{\bar{I}} + \bar{\bar{\tau}}_s\right) : \nabla \vec{v}_s + \nabla \cdot \left(k_\Theta \nabla \Theta\right) - \gamma_\Theta - 3K_{gs}\Theta\right) \tag{7}$$

Equations (4), (6) and (7) can refer to either the white (s_1) or the black (s_2) solids phases. As can be seen in Eq. (6), the extra term $\vec{f}_{fric}$ is incorporated to account for the effect of the front and back walls of the pseudo-2D bed in an analogous way to Hernández-Jiménez et al. (2016). This extra term has been neglected for the gas phase since it is expected to have a comparatively minor effect. Further details about the implementation of this term can be found in Hernández-Jiménez et al. (2016). However, the friction term needs a slight modification as a consequence of incorporating two solids phases.

To correctly implement the extra term, $\vec{f}_{fric}$, in the two solid phases, it should be scaled with the relative amount of solids in each cell:

$$\vec{f}_{fric} = \frac{2c\vec{v}_s}{Z}\frac{\alpha_s}{\alpha_{\max}} \tag{8}$$

Where Z is the bed thickness, c is the particle-wall interaction coefficient calculated experimentally by Hernández-Jiménez et al. (2013), α_s is α_{s1} or α_{s2} depending on the solid phase that refers to $\vec{f}_{fric}$ and $\alpha_{\max}$ is the maximum solid fraction that can be encountered in a computational cell, which is 0.6 if a void fraction of 0.4 is considered in the dense bed.

The simulation campaign includes standard two-fluid model simulations without including the extra friction term and two-fluid model simulations including it.

Regarding the numerical simulations, a second order accurate scheme was selected to discretize the convective derivatives of the governing equations. The distributor was modelled as a uniform velocity inlet and a fixed pressure boundary condition was chosen at the top of the freeboard. The lateral walls of the bed were modelled as no-slip boundary condition for the gas and solid phases. Each of the solids phases are initially placed at both sides of the bed similarly to the experimental procedure. The particle diameter used to model the dense phase in the simulations was equal to the average particle diameter in the corresponding experiment and the same density. The angle of internal friction was set to $\phi = 30$ deg, which is related to the Coulomb's coefficient of friction through $\tan\phi = \mu$. The inter-particle coefficient of restitution was $e_s = 0.9$, the gas density was $\rho_g = 1.2$ kg/m^3 and the gas viscosity was $\mu_g = 1.8 \cdot 10^{-5}$ Pa·s.

RESULTS & DISCUSSION

This section firstly analyzes the suitability of the two-fluid model incorporating the wall friction model to predict the mixing process. This is done by comparing the simulations with the friction term with experiments and numerical results obtained from the standard two-fluid model simulations without including it.

Fig. 2 shows several snapshots of the experiments (top) and the numerical simulations including the friction term (bottom). As the mixing process progresses, the white particles vanish in the mixture of particles, making the white area detected by the DIA processing to gradually decrease. The simulation results are exported to greyscale images where only one of the solid phases is represented as white. Then, the volume fraction (α_s) of this solid decreases as the bed mixes analogously to the white area detected in the experiments. Therefore, the white area recognition in the simulations represents almost the same process as in the experiments.

As can be observed, a fairly good qualitative agreement is found between the experimental results and the simulations when the frictional term is considered. Both black and white particles start to mix at a time around 2 seconds. At 6 seconds some remaining clusters of unmixed particles can be seen. After approximately 8 seconds, a randomly mixed state is achieved in which mixing reaches a maximum (i.e. MI stabilizes around a value equal to 1).

To quantitative describe the mixing process, Fig. 3 shows the time evolution of the previously defined Mixing Index (Eq. 1), for the experimental results and the simulations. The same data processing methodology applied to the experimental images is used in the numerical snapshots to make the comparison consistent.

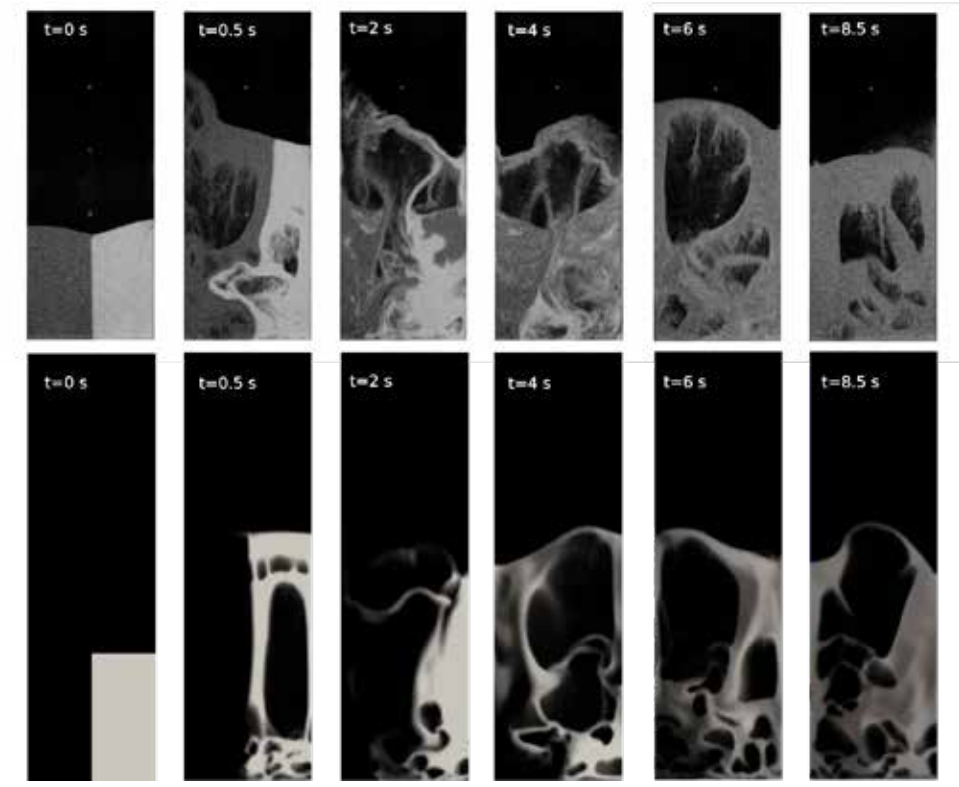

Fig. 2: Example of a mixing process: snapshots of the experimental bed (top) and snapshots of the simulation results including the friction model (bottom). Particle size = 0.6-0.8 mm, U_0/U_{mf} = 2.5.

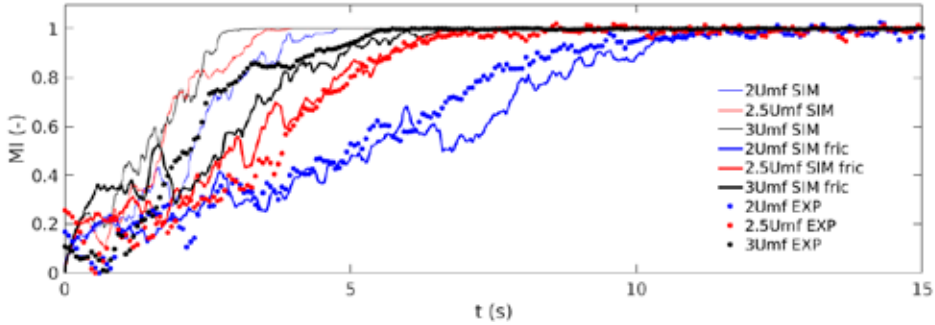

Fig. 3: Time evolution of the Mixing Index (Eq. 1) for the experimental results and the numerical simulations with and without the friction term. Particle size = 0.6-0.8 mm.

First, it is noticeable the differences between the simulations with the wall friction term and without it. The slope of the curve in the cases without the friction term is much higher than in the simulations including it and in the experimental results. The slope of increasing MI in the experiments is quite similar to the simulation results with the friction term. Also, the time where the randomly mixed state is achieved (i.e. MI = 1) in the experiments is also quite similar to the simulations with the friction term, obtaining substantially lower mixing times (time to approach MI = 1) when the friction is neglected in the simulations.

To characterize the mixing time, Fig. 4 shows t_{95} versus the excess gas velocity. t_{95} is defined as the time when the mixing index of Eq. (1) reaches a value of 0.95. The fitting ($t_{95} = 5.42(U_0 - U_{mf})^{-0.72}$) obtained

from the experimental results, which was linked with the lateral dispersion coefficient by Sánchez-Prieto et al. (2017), is also included in the figure.

Overall, it can be observed that the inclusion of the friction term in the simulations improves the prediction of the numerical results when compared with the experimental findings. In general, a reasonable deviation of the simulation results including the friction term from the fitting line is obtained in comparison with the experimental results. Discrepancies between the experimental and numerical results seems to grow at low superficial gas velocities for the small and big particle sizes. Besides, the experimental trend is better reproduced by the simulations when using the friction model. The results of the simulations without the friction term show a systematic under-prediction of the mixing time, especially for the medium and small particle sizes. This is in agreement with Hernández-Jiménez et al. (2016), who showed that the inclusion of the friction term slows down the overall motion of solids and bubbles, which implies a lower mixing rate.

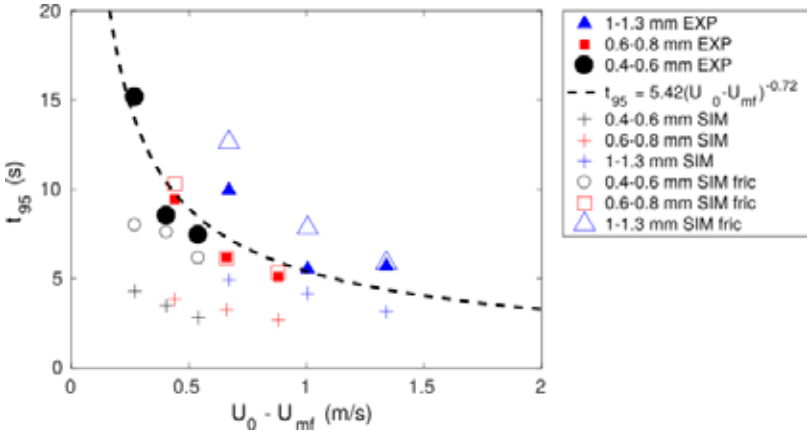

Fig.4: Mixing time, t_{95}, as a function of the excess gas velocity, U_0-U_{mf}.

Therefore, the simulation results can be used to extract more detailed information than that of the experiments. The volume fraction of the two solid phase as well as the gas volume fraction on each computational cell can be extracted from the simulations to perform a more detailed analysis of the mixing process. Thus, a new Mixing Index (MI*) can be calculated by comparing the solids volume fraction of each solids phase on every cell at each time instant. This new Mixing Index (MI*) computes the number of mixed cells in the bed divided by the total number of cells occupied by solids. A cell is considered to be mixed if the difference between the volume fraction of the two solids phases is below a threshold:

$$MI^* = \frac{N_{mixed}}{N_{total}} \tag{9}$$

where N_{total} is the initial total number of cells that are occupied by solids, and N_{mixed} is defined as follows:

$$\begin{aligned} &N_{mixed} = 1 \quad \text{if} \quad \alpha_{s,1}(1-th) < \alpha_{s,2} < \alpha_{s,1}(1+th) \quad \& \quad \alpha_g < 1 \\ &N_{mixed} = 0 \quad \text{otherwise} \end{aligned} \tag{10}$$

Fig. 5 shows the mixing curves obtained for different values of the threshold, 0.2, 0.1 and 0.05, for the medium size particles and an excess gas velocity of U_0-U_{mf} = 0.66 m/s, for the simulation results using the friction model. The figure presents only the simulation results that incorporate the friction model because they were shown to give a better prediction of the experimental findings.

It can be seen how the mixing time defined previously, t_{95}, strongly depends on the threshold selected to consider that a cell is mixed. Reducing the value of this threshold, the new Mixing Index (Eq. 9) tends to the original Mixing Index (Eq. 1). The main difference between MI and MI* is that MI takes can only distinguish one solids phase but the information from the gas phase and the other solids phase is missing. So that, variations of the gas volume fraction in the dense bed are neglected. In the simulation results, information about the three phases can be extracted and the balance from Eq. (2) is fulfill. In the experiments, the mixing time is slightly underestimate because the second solid phase cannot be distinguishable from the gas phase. So, a cell can be considered mixed in the case that it is occupied by white solids and gas. On the

other hand, MI*, represents a more accurate procedure to discriminate if a cell is mixed thanks to the level of detail of the simulation solution.

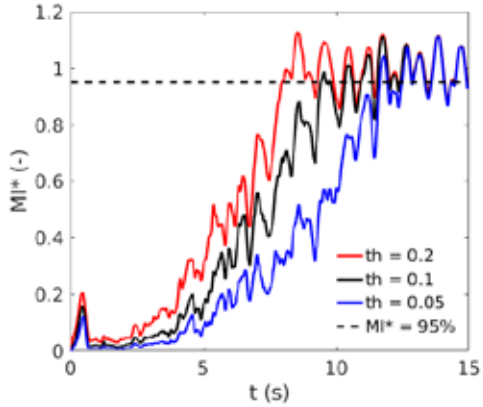

Fig.5: Time evolution of the new Mixing Index (Eq. 9) for the simulation results with the friction term. Particle size = 0.6-0.8 mm. U_0/U_{mf} = 2.5.

Finally, Fig. 6 shows the mixing time, t_{95}*, of the new Mixing Index, MI*, as a function of the excess gas velocity for different values of the threshold used to consider mixing. The figure shows again that different values of the mixing time are found when the threshold selected changes. Besides, noticeable differences appear when this is compared to the original t_{95}. The new mixing time, t_{95}*, is not only dependent on the excess gas velocity, but it seems to be more sensitive to the particle size of the bed material. Furthermore, a decrease of the mixing time is typically found with the excess gas velocity. This decrease with the particle diameter is higher for the smaller particles.

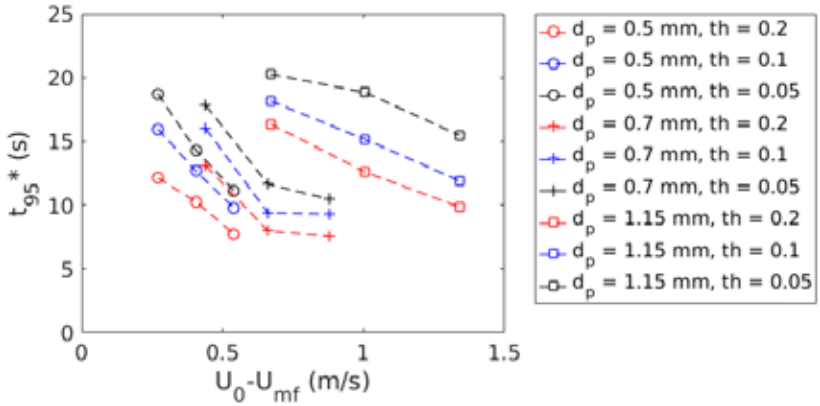

Fig.6: Mixing time, t_{95}*, as a function of the excess gas velocity, U_0-U_{mf}, for the simulation results with the friction term.

CONCLUSIONS

The present work has studied the different mixing mechanisms in fluidized beds by means of numerical simulations. The numerical results were compared with the experimental results obtained in a pseudo-2D fluidized bed that allows optical access to the interior of the system through the frontal glass wall. The prediction of the numerical simulations was improved by incorporating a friction model that accounts for the effect of the front and rear walls in the pseudo-2D bed without the need to incorporate such walls in the simulation domain. Furthermore, the simulations were employed to analyze the mixing in the fluidized bed in more detailed as they provide information about the two solid phases and the gas phase. This new mixing time decreases with the excess gas velocities with different decreasing rates depending on the particle size.

NOTATION

α gas or solids concentration, -
$A_{w,i}$ white area recognized in each image, px^2
$A_{w,max}$ maximum white area recognized, px^2
c particle-wall interaction coefficient, $kg/(m^2s)$
e_s coefficient of restitution, -
d_p particle diameter, mm
f_{fric} friction force, N
γ_θ collisional dissipation of Θ, m^2/s^2
g gravity, m/s^2
H_0 static bed height, m
Θ granular temperature, m^2/s^2
K_{gs} drag force between gas and solids, $kg/(m^3s)$
K_θ diffusion coefficient for granular energy, kg/(ms)
MI mixing index, -
MI* new mixing index, -
N_{mixed} number of computational cells mixed, -
N_{total} total number of computational occupied by solids, -
ρ density, kg/m^3
τ stress tensor, Pa
t time, s
t_{95} time needed to reach 0.95MI, s
t_{95}* time needed to reach 0.95MI*, s
th threshold to discriminate a mixed cell, -
μ_g gas viscosity, Pa·s
U_0 superficial gas velocity, m/s
U_{mf} minimum fluidization velocity, m/s
v velocity, m/s
W bed width, m
Z bed thickness, m

REFERENCES

Benyahia, S., Syamlal, M., O'Brien, T.J. Summary of MFIX Equations 2005-4, 2007.

Hernández-Jiménez, F., Sánchez-Prieto, J., Soria-Verdugo, A., Acosta-Iborra, A. Experimental quantification of the particle–wall frictional forces in pseudo-2D gas fluidised beds. Chem. Eng. Sci., 102 (2013), pp. 257–267.

Hernández-Jiménez, F., Cano-Pleite, E., Sánchez-Prieto, J., Garcia-Gutierrez, L.M., Acosta-Iborra, A. Development of an empirical wall-friction model for 2D simulations of pseudo-2D fluidized beds. Advanced Powder Technology, 27 (2016), 521-530.

Lacey, P.M.C. Developments in the theory of particle mixing. Journal of Applied Chemistry, 4:257-268, 1954.

Otsu, N. A threshold selection method from gray-level histograms. IEEE Trans. Syst. Man Cybern., 9 (1979), pp. 62–66.

Rhodes, M.J., Wang, X.S., Nguyen, M., Stewart, P., Liffman. K. Study of mixing in gas-fluidized beds using DEM model. Chemical Engineering Science, 56(8) (2001), 2859-2866.

Sánchez-Prieto, J., Hernández-Jiménez, F., Garcia-Gutierrez, L-M., Soria-Verdugo, A. Experimental study on the characteristic mixing time of solids and its link with the lateral dispersion coefficient in bubbling fluidized beds. Chemical Engineering Journal 307 (2017), 113–12.

Syamlal, M., Rogers, W., O'Brien, T.J., MFIX Documentation: Theory Guide, U.S. Department of Energy (DOE), Morgantown Energy Technology Center, Morgantown, West Virginia, 1993.